

Design of Experimental Regenerative Braking Simulation System and Experimental Research

Ping Xu*, Zongzheng Ma +1, and Yuelong Yuan#

www.rericjournal.ait.ac.th

ARTICLE INFO

Article history: Received 27 April 2025 Received in revised form 22 September 2025 Accepted 09 October 2025

Keywords: Energy recovery efficiency Braking distance Regenerative braking system Simulation test bench STM32 microcontroller

ABSTRACT

To address the limitations of real-vehicle regenerative braking systems, such as high experimental costs, difficult data visualization, and inadequate support for experimental education, this study developed a parallel hydraulic regenerative braking simulation test bench and conducted systematic experimental research. The test bench integrates three core subsystems: an inertia simulation system, a kinetic energy recovery system, and a control system. Controlled-variable experiments were carried out to analyze the effects of two key parameters, initial flywheel rotational speed and hydraulic pump displacement, on system performance, including braking distance, energy recovery efficiency, and energy reuse efficiency. Experimental results showed that: (1) Braking distance increased with initial speed regardless of pump displacement; (2) Energy recovery efficiency first increased and then decreased with initial speed, reaching a maximum of 58.9% at 35 km/h, and was positively correlated with pump displacement; (3) Energy reuse efficiency peaked at 35% when the flywheel initial speed was 34.9 km/h and increased with pump displacement, reaching 22% at 25 mL/r). This research offers experimental support for parameter matching and performance improvement of hydraulic regenerative braking systems.

1. INTRODUCTION

Hydraulic systems are widely employed as power sources in heavy-duty vehicles and construction machinery, such as hydraulic hybrid propulsion and hydraulic hybrid buses, which are used to drive the vehicles themselves or their associated mechanical equipment [1]-[3]. The integration of regenerative braking technology offers dual benefits: it not only helps reduce wear on brake components [4]-[5], but also converts the vehicle's kinetic energy during braking into other usable forms of energy, which can then be stored in energy storage devices for reuse. Compared with other types of braking energy recovery systems, hydraulic energy recovery systems provide high output power, rapid response, flexible control performance, and reliable operation. Thus attracting increasing attention.

Pourmovahed (1992) from the University of Wisconsin pioneered an analytical framework for hydraulic systems encompassing motors accumulators, which laid a theoretical foundation for

DOI: https://doi.org/10.64289/iej.25.0412.2974222

Corresponding author;

E-mail: zongzhengma@haue.edu.com

subsequent simulation studies of hydraulic hybrid powertrains [6]. A decade later, Filipi (2004) at the University of Michigan developed a vehicle powertrain simulation platform tailored for hybrid vehicle research, introducing both rule-based energy management strategies and dynamic programming-based global optimization algorithms [7]. Significant industrial advancement emerged in 2016 with Dana Holding Corporation's Spicer Power Boost system, which demonstrated the capability to recover kinetic energy and redirect it for vehicle propulsion, achieving up to 45% fuel economy improvement in operational testing [8]. Academic contributions continued with Ding et al. (2019) from Zhejiang University, whose field trials on heavy-duty engineering vehicles reported a 31.2% reduction in fuel consumption through their parallel hybrid configuration [9]. Zhang et al. From Shanghai Jiao Tong University (2020) further validated the technology in urban transit applications, recording over 25% fuel savings and a 35% reduction in particulate emissions under real-world conditions [10]. Most recently, Wang et al. (2022) from Shandong University of Technology proposed a novel parallel hydraulic hvbrid architecture incorporating compound accumulators, achieving a 31.2% fuel economy improvement over conventional buses in simulated Chinese urban driving cycles [11]. Collectively, these findings underscore the potential of hydraulic regenerative braking systems to concurrently enhance vehicle energy efficiency, power performance, and emission characteristics.

^{*}School of Civil Engineering, Henan University of Engineering, Zhengzhou 451191, China.

⁺School of Mechanical Engineering, Henan University of Engineering, Zhengzhou, 451191, China.

^{*}School of Intelligent Mechanical and Electrical Engineering, Zhongyuan University of Technology, Zhengzhou, 450007, China.

The hydraulic regenerative braking system's core components include the hydraulic pump/motor assembly and energy storage accumulator. Zhou (2013) demonstrated that pump displacement constitutes a key factor influencing energy recovery efficiency, with dynamic modulation of pump/motor displacement enabling precise control over vehicle braking force characteristics [12]. In a complementary study, Zhang (2015) analyzed fluid mixing dynamics and proposed substituting a single large accumulator with a dual smaller accumulator configuration to optimize system responsiveness [13]. Subsequently, Xu (2018)conducted a simulation analysis and demonstrated that the braking torque of the system exhibits a linear relationship with the accumulator pressure, indicating that this configuration can effectively enhance the energy recovery efficiency [14]. To further analyze the influence of accumulator parameters on system performance, Wang (2022) investigated the accumulator characteristics and revealed that the precharge pressure of the accumulator plays a critical role in both the duration of efficient charging and the overflow volume in the energy recovery system. An appropriate precharge pressure was shown to achieve an energy utilization rate of 67.43% [15]. Zhang's (2023) parametric analysis revealed that accumulator volume and air compressor displacement exert significant influence on system performance. Specifically, increasing accumulator volume was found to enhance energy regeneration efficiency by 18-22%, while compressor displacement demonstrated a nonlinear relationship with system efficiency under varying load conditions [16]. Most recently, Gao (2025) analyzed the system by altering the vehicle's driving modes and demonstrated that this control strategy can achieve an energy recovery efficiency of 78% and improve fuel economy by 24.34% [17].

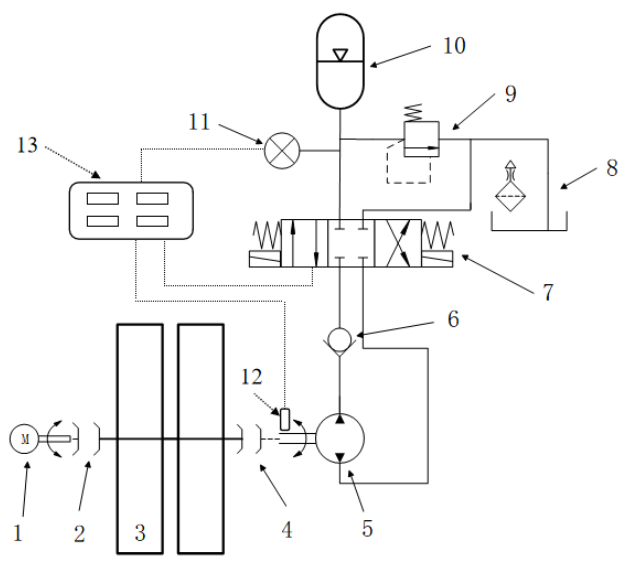
Demonstrating the principles of the brake energy recovery system and conducting experimental tests are of great importance. However, using a real vehicle equipped with a regenerative braking system for such purposes poses significant challenges. First, the brake energy recovery system is integrated into the vehicle controller, precluding direct data display. Second, the costs associated with utilizing an entire vehicle are also substantial. To address these issues, a simulation test bed for the regenerative braking system has been developed based on the working principles of the hydraulic regenerative braking system. This test bed offers three key advantages: it fulfills the dual functions of "teaching demonstration" and "experimental research," features low costs thanks to the STM32 single-chip microcomputer as its main controller, and enables flexible parameter adjustment.

This paper is structured as follows: Section 2 details the design of the regenerative braking test bed; Section 3 presents experimental applications based on the designed test bed; and Section 4 draws conclusions.

2. DESIGN OF THE REGENERATIVE BRAKING TEST BED

2.1 Principle of the Regenerative Braking Test Bed

The hydraulic regenerative braking test bed is illustrated in Figure 1, comprising three core subsystems: an inertia simulation system, a kinetic energy recovery system, and a control system. The inertia simulation system is designed to replicate the inertial characteristics of a vehicle, with an electric motor and a flywheel assembly. The kinetic energy recovery system is responsible for converting the kinetic energy of the flywheel into hydraulic energy, including a hydraulic pump/motor, an electromagnetic directional valve, an accumulator, and a relief valve. The control system is used to regulate actuator operations and sample data, which is composed of two electromagnetic clutches, one electromagnetic directional valve, one speed sensor, one pressure sensor, and one control unit.



1. Motor; 2. Electromagnetic clutch A; 3. Flywheel group; 4. Electromagnetic clutch B; 5. Pump; 6. One-way valve; 7. Three-position four-way electromagnetic directional valve; 8. Tank; 9. Relief valve; 10. Accumulator; 11. Pressure sensor; 12. Speed sensor; 13. Control unit

Fig. 1. Diagram of the regenerative braking test bed.

2.2 Flywheel Group Design

In order to simulate a vehicle with a total mass of 145kg, a tire radius of 0.2m, and a maximum speed of 50km/h, a flywheel group is used. The relationship between the kinetic energy of the vehicle and the rotation of the flywheel is expressed as follows:

$$\frac{1}{2}J_c \omega_1^2 = \frac{1}{2}J_c (3.6n_1)^2 = \frac{1}{2}m (3.6n_2 r)^2$$
 (1)

where the flywheel moment of inertia is denoted by J_c (kg·m²), the angular velocity of the flywheel is denoted by ω_1 (rad/s), the simulated vehicle mass is denoted by m (kg), , the rotational speed of the flywheel is denoted by n_1 (r/min), the rotational speed of the simulated vehicle is denoted by n_2 (r/min), the angular velocity of the simulated vehicle is denoted by ω_2 (rad/s), and the tire radius of the simulated vehicle is denoted by r (m).

The maximum rotational speed of the flywheel is set at 1325r/min, which is twice that of the simulated vehicle. Consequently, the calculated moment of inertia for the flywheel is 1.5 kg·m², and the total moment of inertia of the flywheel set must exceed this value. To meet this requirement, the flywheel assembly comprises two flywheels cast from HT200, each with a mass of 70 kg, a diameter of 0.45m, and a thickness of 0.1m.

2.3 Motor Selection

Given that the flywheel group does not require high acceleration, the acceleration process is set to be completed within 30s. This means the flywheel group reaches 1325r/min (maximum rotational speed of the flywheel group) in 30s, so the angular acceleration of the flywheel set is calculated as follows:

$$\frac{d\omega}{dt} = \frac{\Delta\omega}{\Delta t} = \frac{2\pi \times 1325}{60 \times 30} = 4.62 \,\text{rad/s}^2 \tag{2}$$

Then the motor torque is calculated as follows:

$$T = J_c \frac{d\omega}{dt} = 1.6 \times 4.62 = 7.39 \,\text{N} \cdot \text{m}.$$
 (3)

And the motor required power is calculated as follows:

$$P = \frac{T \times n}{9550} = \frac{7.39 \times 1325}{9550} = 1.1 \text{kW}.$$
 (4)

It is a common engineering recommendation to select a motor with a rated power ranging from 1.1 to 1.5 times the load power. Based on the aforementioned calculations, a three-phase alternating current (AC) motor, model YS-90L-6, was chosen, with a rated power of 1.5kW, a rated voltage of 380V, and a rated torque of 9.8N • m.

2.4 Hydraulic Pump Selection

In accordance with relevant standards, when a vehicle's initial speed is 50km/h, its braking distance shall not exceed 21m. Assuming the braking process follows a uniform deceleration pattern, the braking deceleration can be calculated using Formula (5):

$$a = \frac{v^2}{2s} = \frac{(50/3.6)^2}{2 \times 21} = 4.6 \text{m/s}^2$$
 (5)

where the braking deceleration is denoted by a (m/s²), the braking distance is denoted by s (m). So the braking torque is calculated as follows:

$$T_m = mar = 150 \times 4.6 \times 0.2 \approx 137.8 N \cdot m.$$
 (6)

When all braking force is provided by the regenerative braking system, the required torque of the hydraulic pump can be calculated using Formula (7), with frictional and air resistance neglected.

$$T_p = \frac{i \times q \times p_a}{2\pi \times \eta} = \frac{1.28 \times q \times p_a}{2 \times \pi \times 0.95} \approx 0.43 \, qp_a \tag{7}$$

where the main reducer ratio is denoted by i and the value is 1.28 according the real car, the hydraulic pump working pressure is denoted by p_a (MPa;), the hydraulic pump displacement is denoted by q (mL/r), the hydraulic pump efficiency is denoted by η and equals 0.95 according to real vehicle specifications.

The torques calculated via Formulas (6) and (7) should be equal; based on this equality, the product of the hydraulic pump's operating pressure and displacement can be derived using Formula (8).

$$q p_a = 320 \text{N} \cdot \text{m}. \tag{8}$$

So a gear pump model CBN-F316 was ultimately selected, featuring a displacement of 16mL/r, a rated operating pressure of 20MPa, a head of 120m, a volumetric efficiency of 85%, and a rated flow rate of 16L/min. To satisfy the braking torque requirements, the minimum operating pressure of this hydraulic pump must be 8.5MPa.

2.5 Accumulator Selection

To achieve energy recovery, the accumulator must fully absorb the vehicle's kinetic energy during maximum-speed braking. During braking, the braking resistance generated by the hydraulic pump is significantly greater than the rolling resistance and rolling resistance, which can be neglected. The amount of regenerative energy that the accumulator should store can be calculated using Formula (9).

$$E_r = \frac{1}{2} \delta m_{car} v_0^2 = -\frac{P_0 V_0}{n-1} \left[\left(\frac{P_0}{P} \right)^{\frac{n-1}{n}} - 1 \right], \tag{9}$$

Where the energy stored by accumulator is denoted by E_r (J), the mass conversion coefficient is denoted by δ and is set as 1.04, the pre-charge pressure of the accumulator is denoted by P_0 (Pa), the initial volume of the accumulator is denoted by V_0 (m³), the final pressure of the accumulator is denoted by P (Pa), the gas variable coefficient is denoted by P and the value is set as 1.4, the maximum speed of the vehicle is denoted by V_0 (m/s), the mass of the vehicle is denoted by P (kg).

An accumulator with a volume of 4 L is required, given a pre-charge pressure of 8.5MPa and a rated operating pressure of 20MPa based on the Formula (9). To incorporate safety factors, an additional volume of accumulator is necessary during energy recovery, a bladder accumulator, model NXQ-5.0-L, was selected, which has a volume of 5 L and a maximum pressure of 31.5MPa.

2.6 Control System Development

To ensure the proper functionality of the test bed, a dedicated control system has been developed. This system integrates four core parts, signal acquisition, a main controller, actuation components, and a display module, with their configuration schematically illustrated in Figure 2.

(1) Main controller selection

A STM32F103VET6 is selected as the main controller, which features a 32-bit ARM architecture, a 72MHz main frequency computing capability, a dual-channel 12-bit precision analog-to-digital conversion module, 4 channels pulse signal processing functionality, and 4 groups of programmable digital output ports. Therefore, it is capable of sampling real-time voltage/current sensor data, realizing rotational speed monitoring, and controlling actuators such as electromagnetic clutches.

(2) Signal acquisition part design

The signal acquisition module comprises a speed sensor, a pressure sensor, and their corresponding processing circuits. Consequently, the design work encompasses two core aspects: first, the selection of the speed sensor and accumulator pressure sensor; second, the design of the processing circuits.

To measure speed, a high-precision incremental encoder (model: LQ-SDZ512) is selected. It is coaxially mounted on the flywheel to ensure synchronous rotation. The encoder is then wired to the PA0 and PA1 pins of the main controller. By configuring these two pins to timer encoder mode, the square wave signals output by the encoder can be read directly by the main controller.

To measure the accumulator pressure, a PCM300 pressure sensor is employed, which has a maximum measurable pressure of 40MPa, a 24V power supply, and a voltage output range of 0-5V. To convert the current signal into a voltage signal readable by the main controller, a pressure measurement circuit with high-precision sampling resistor is designed that converts the 4-20mA current signal into a corresponding 0.6-3V voltage signal, as illustrated in Figure 3.

Once the current signal is converted to voltage signal, the main controller's built-in A/D peripheral is employed to read the data. The accumulator pressure can then be derived through subsequent calculation.

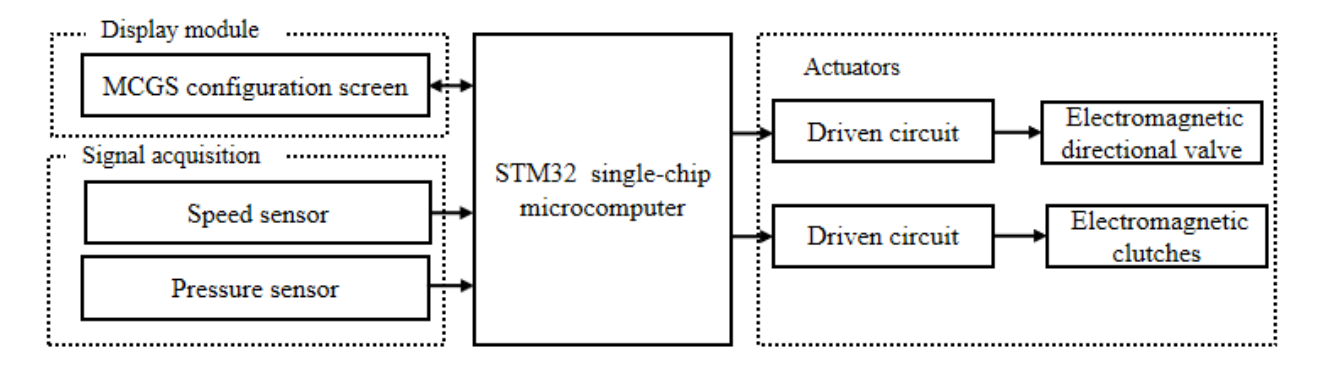


Fig. 2. Diagram of control system of the test bed.

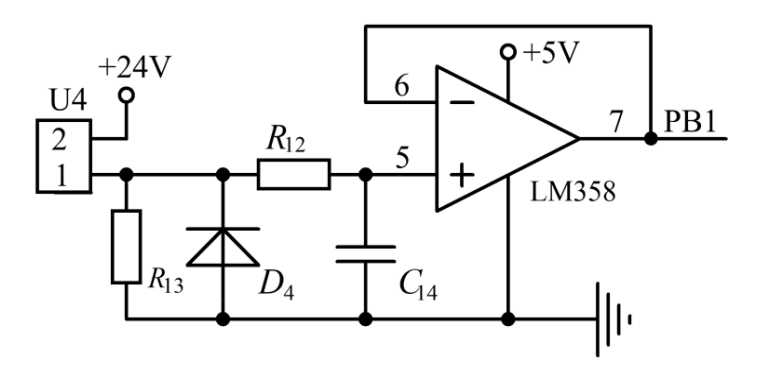


Fig. 3. Circuit of pressure sensor measurement.

(3) Actuator driven circuit design

To control the electromagnetic clutches and directional valve, a dedicated drive circuit has been developed. This drive circuit employs the dual-channel low-voltage driver chip IR4427 to regulate the field-effect transistor (FET) STN4186-whose maximum operating parameters

reach 40V/20A-thereby achieving the required driving function and fully meeting the system's drive specifications as illustrated in Figure 4.

The components labeled Q1 and Q2 correspond to the STN4186 FETs. Meanwhile, a freewheeling diode is integrated into the design to prevent component damage caused by excessive current in the circuit during poweroff. The control pins of the electromagnetic clutches are connected to the RELAY1 and RELAY2 ports. When the main controller outputs a high level via its control pin, the driver chip amplifies this signal and triggers the STN4186 to turn on, placing the electromagnetic clutches in an engaged state. Conversely, when the main controller outputs a low level, the STN4186 remains off, and the clutches switch to a disengaged state.

The control circuit configuration and operational principle for the directional valve are identical to those of the electromagnetic clutches, so detailed elaboration is omitted here.

(4) Computer Interface Design

The Host Message Interface is based on the MCGS configuration screen and it communicates with the controller through the Modbus protocol. It can change the logical values of parameters, the states of the electromagnetic clutches, electromagnetic directional valves which can change the state of the test bed into energy recovery or energy release. In addition, the maximum speed of the flywheel group and the

displacement can also be set through the interface which is shown in Figure 5.

The interface supports four core functional modules: first, for logic parameter modification, users can adjust the threshold values governing system operation to flexibly adapt to different working scenarios; second, in terms of actuator state control, it enables real-time switching of the engagement status of electromagnetic clutches and the configuration of directional valves, thereby toggling the system between energy recovery mode and energy release mode; third, regarding operational parameter programming, users can input settings for key operational parameters-including the maximum flywheel rotational speed and pump displacement-through configurable dialogues; fourth, providing real-time visualization of metrics, specifically including flywheel angular velocity, accumulator pressure, and status indicators for system energy flow.

(5) Software Design

The experiment process control system follows the workflow illustrated in Figure 6.

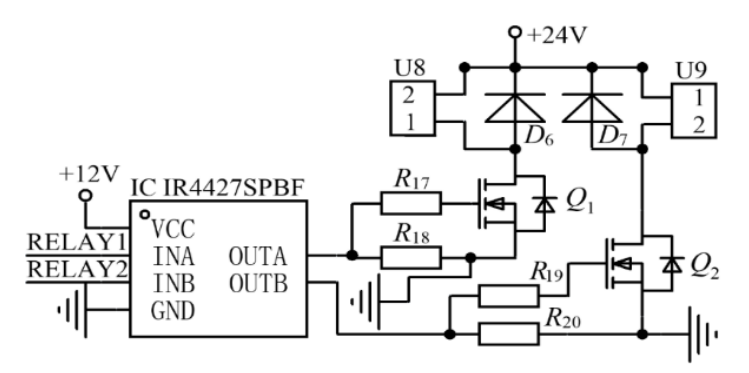


Fig. 4. Drive circuit of electromagnetic clutches.

Regenerative braking simulation test bench

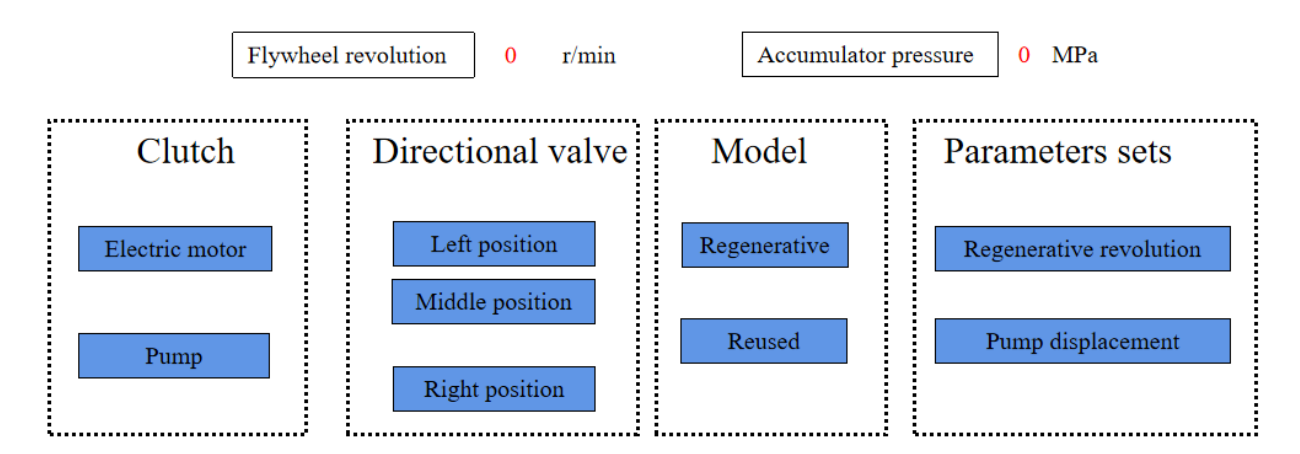


Fig. 5. Host message interface.

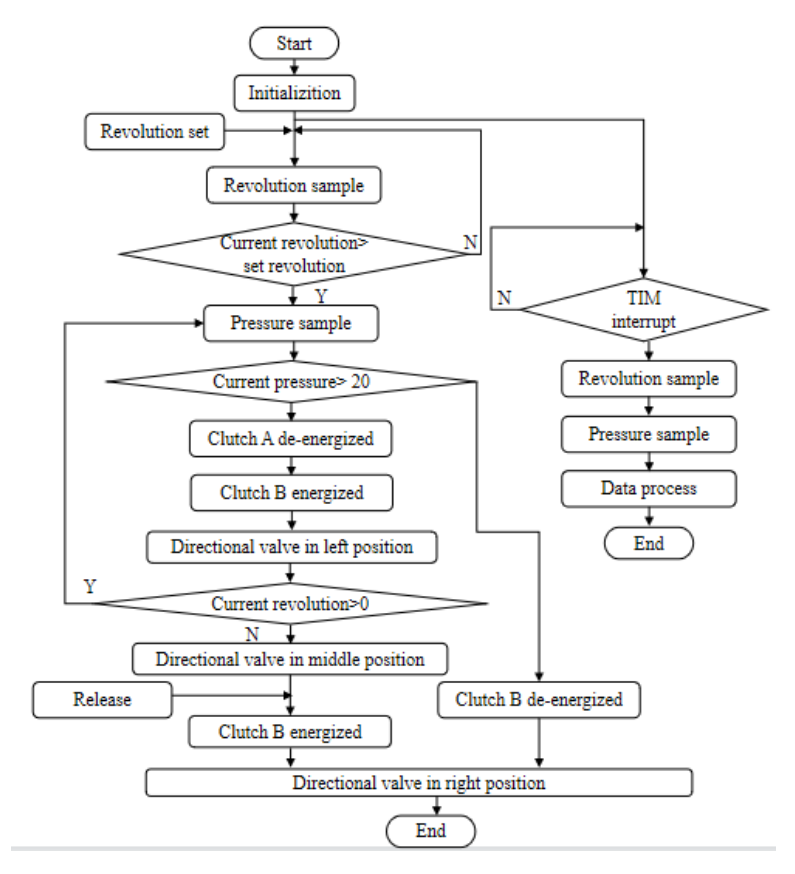


Fig. 6. Flow chart of the control system.

Once the program is activated, an initialization process is initiated, encompassing parameter settings, channel configurations, storage path designation, calibration equations, and sampling parameter configurations. Subsequently, the motor and the relay controlling electromagnetic clutch A is energized to drive the flywheel assembly manually. When the flywheel assembly reaches the preset rotational speed, electromagnetic clutch 1 is deenergized to disconnect the motor from the flywheel assembly, while electromagnetic clutch B is energized to engage the flywheel with the hydraulic pump. Concurrently, the accumulator pressure and flywheel assembly speed are continuously collected and displayed in real time. While the rotational speed remains non-zero, the hydraulic pump operates continuously, and the energy recovery process persists. The energy recovery process terminates when either the accumulator pressure exceeds the preset threshold, the flywheel speed drops to zero, or the accumulator pressure reaches the specified limit of 31 MPa.

The physical test bench is illustrated in Figure 7. After the bench was fully set up and the control program underwent thorough debugging to confirm operational stability, the test system was ready for operation.



Fig. 7. Test bed.

3. EXPERIMENTAL RESEARCH

To verify the performance of the designed hydraulic regenerative braking simulation test bed and identify the key factors influencing the system's energy recovery and reuse, this study conducted controlled-variable experiments focusing on two core parameters: the initial rotational speed of the flywheel (corresponding to vehicle driving speed) and the displacement of the hydraulic pump. By testing the braking distance, energy recovery efficiency, and energy reuse efficiency under different working conditions, the effect of these parameters on system performance was revealed, providing experimental basis for the parameter optimization and practical application of hydraulic regenerative braking systems.

3.1 Experimental Scheme Design

3.1.1 Experimental variables and control conditions

The controlled-variable method was adopted in this experiment to explore the effects of the initial rotational speed of the flywheel and the displacement of the hydraulic pump respectively. The basic experimental conditions and variable settings are as follows:

(1) Fixed experimental conditions:

The hydraulic pump model is CBN-F316 (rated pressure 20 MPa, volumetric efficiency 85%), and the accumulator model is NXQ-5.0-L (volume 5L, precharge pressure 8.5MPa, maximum pressure 31.5MPa). The control logic of the electromagnetic clutches and directional valve is executed by the STM32F103VET6 microcontroller according to the preset program. The data sampling frequency is 10 Hz, and the experimental ambient temperature is maintained at 25±2°C.

(2) Variable 1: Initial rotational speed of the flywheel: Based on the conversion relationship between flywheel speed and vehicle speed, the flywheel speed was gradually increased from 13.5km/h to 50km/h (corresponding to flywheel speeds adjusted accordingly). The displacement of the hydraulic pump was fixed at 16mL/r to test the braking distance, energy recovery efficiency, and energy reuse efficiency under different initial speeds.

(3) Variable 2: Displacement of the hydraulic pump: The initial rotational speeds of the flywheel were fixed at 50km/h and 40km/h, and the displacement of the hydraulic pump was set to four gradients: 10mL/r, 15mL/r, 20mL/r, and 25mL/r. The braking distance and energy efficiency indicators under different displacements were tested.

3.1.2 Evaluation indicators

Three core indicators were used in the experiment to quantify the system performance, and the calculation formulas were derived based on the principle of energy conservation and the characteristics of the hydraulic system:

1. Braking distance: Refers to the theoretical driving distance of the vehicle when the flywheel decelerates from the initial speed to 0, which reflects the braking performance of the system as shown in Equation (10). It

is calculated by collecting the flywheel speed in real time and combining it with the vehicle dynamics model.

$$n_1 = 60 \cdot v / (2 \cdot 3.14 \cdot 0.1 \cdot 3.6)$$
 (10)

2. Energy recovery efficiency: Defined as the ratio of the hydraulic energy actually stored in the accumulator (E_r) to the initial kinetic energy of the flywheel (E_{car}) . The calculation formula is shown in Equation (11).

$$\eta = \frac{E_r}{E_{car}} = -\frac{P_0 V_0}{n-1} \left[\left(\frac{P_0}{P} \right)^{\frac{n-1}{n}} - 1 \right]$$
 (11)

3. Energy reuse efficiency: Defined as the ratio of the maximum kinetic energy of the flywheel (E_1) driven by the energy released from the accumulator to the energy stored in the accumulator. The calculation formula is shown in Equation (12).

$$\eta_1 = \frac{E_1}{E_r} = \left(\frac{\omega_3}{\omega_1}\right)^2 = \left(\frac{n_3}{n_1}\right)^2 \tag{12}$$

Where the moment of inertia of group after energy recovery is denoted by E_1 (kg·m²), the rotational angular velocity of flywheel group after energy recovery is denoted by ω_3 (rad/s), the rotational speed of flywheel group after energy recovery is denoted by n_3 (r/min).

3.2 Effect of Initial Flywheel Rotational Speed on System Performance

3.2.1 Effect on braking distance

Figure 8 shows the variation of braking distance under different initial vehicle speeds. As observed from the figure, the braking distance increases significantly with the increase of the initial speed. When the initial speed is 13.5km/h, the braking distance is only 7m while the braking distance increases to 35m when the speed increases to 30km/h. And the value further extends to 55 m when the speed reaches 50km/h.

The pre-charge pressure of the accumulator (8.5 MPa) is relatively low and leads to insufficient braking torque generated by the pump, which cannot rapidly pressurize the hydraulic fluid in the accumulator, thereby prolonging the braking process and making the actual braking distance longer.

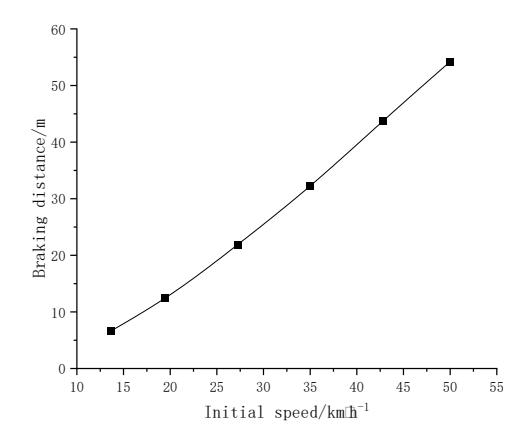


Fig. 8. Braking distance at different initial vehicle speeds.

3.2.2 Effect on energy recovery efficiency

Figure 9 presents the variation of energy recovery efficiency with different initial speeds. As shown in the figure, the energy recovery efficiency exhibits a *first increasing and then decreasing* trend with changing initial speed. The efficiency rises continuously as the initial speed increases when the speed is below 35km/h, reaches a maximum value of 58.9% at 3 km/h, and then shows a gradual downward trend as the initial speed exceeds 35km/h.

This variation trend may be attributed to the combined effects of the dynamic characteristics of the vehicle's energy recovery system, the matching degree between the motor's operating state and speed, and energy loss in the transmission process. At the low-speed stage (< 35km/h), the flywheel rotational speed remains relatively low, resulting in insufficient output pressure and flow from the hydraulic pump. This inadequacy prevents the pump from effectively overcoming the accumulator's pre-charge pressure. Consequently, only a small amount of hydraulic fluid can be pumped into the accumulator, while most of the flywheel's kinetic energy is lost due to internal friction and inefficient energy transfer, ultimately resulting in low energy recovery efficiency. In contrast, at the high-speed stage (>35km/h), the accumulator pressure increases with the rising volume of charged oil. At this point, mechanical losses become more significant as the system approaches its operational limits. Slight slippage may occur between components, reducing the actual input torque to the pump and hindering continuous fluid charging of the accumulator. The excess kinetic energy is then lost in the forms of heat and leakage, thereby causing a decline in energy recovery efficiency.

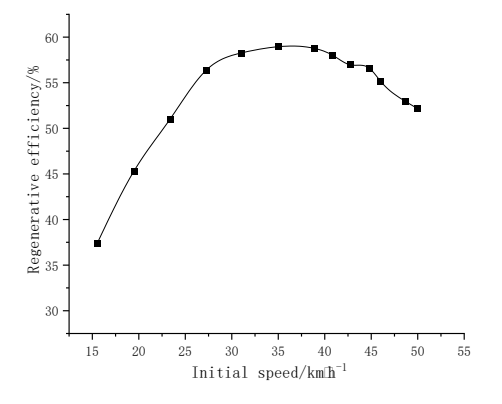


Fig. 9. Regenerative efficiency of different initial speeds.

3.2.3 Effect on energy reuse efficiency

Figure 10 shows the variation trend of the corresponding energy reuse efficiency. The figure demonstrates that the maximum achievable flywheel speed increases with higher initial braking speeds. When the initial speed is 1300r/min (50km/h), the maximum rotational speed of the flywheel driven by the accumulator reaches 672 r/min. The energy reuse efficiency also shows a "first increase and then decrease" trend with the change of the initial speed: when the initial speed is 400 r/min (15.4)

km/h), the efficiency is only 24.5%; when the speed increases to 900r/min (34.9km/h), the efficiency reaches its maximum value of 35%; after that, as the speed continues to increase, the efficiency gradually decreases.

At low speeds, the accumulator stores less energy and cannot provide adequate driving force for the flywheel, so the reuse efficiency is low. And at high speeds, the pressure of the accumulator is too high, which leads to an increase in the braking resistance of the hydraulic pump. The stored energy cannot be fully converted into driving energy, and a portion is dissipated, resulting in a decrease in efficiency.

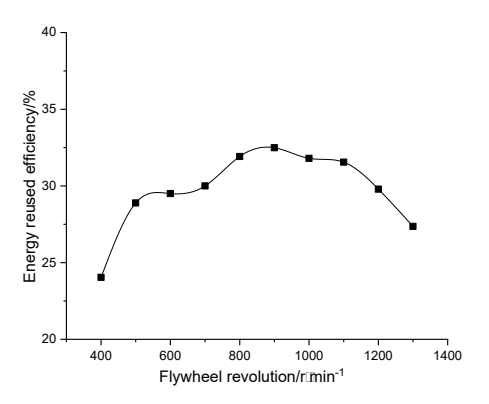


Fig. 10. The energy reused efficiency at different initial speeds.

3.3 Effect of Hydraulic Pump Displacement on System Performance

3.3.1 Effect on braking distance

Figure 11 shows the variation of braking distance under different hydraulic pump displacements (initial speeds are 50km/h and 40km/h respectively). The figure demonstrates that under the same initial speed, the braking distance decreases significantly with increasing the pump displacement. Similarly, When the initial speed is 50km/h, the braking distance at a displacement of 10mL/r is 178m, and it shortens to 65m, representing a decrease of 63.5% when the displacement is 25mL/r. When the initial speed is 40 km/h, the braking distance corresponding to a displacement of 10 mL/r is 110m, and it shortens to 38.8m, with a decrease of 64.7% when the displacement is 25mL/r.

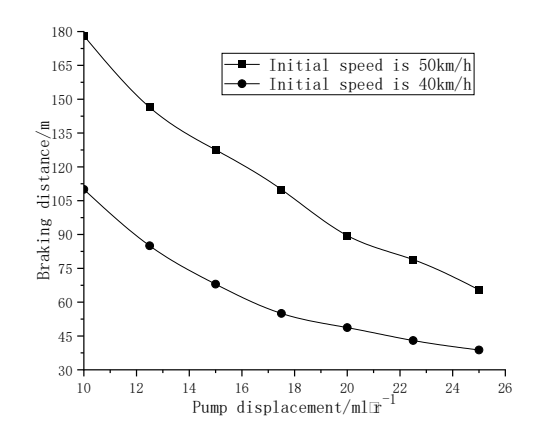


Fig. 11. Braking distance at different pump displacements.

As pump displacement increases, more hydraulic fluid is displaced per unit time, accelerating the accumulator pressurization and enhancing the conversion efficiency from kinetic to hydraulic energy. Consequently, the braking process is shortened, resulting in reduced braking distance.

3.3.2 Effect on energy recovery efficiency

Figure 12 shows the variation of energy recovery efficiency with the pump displacement when the initial speed is 50km/h (flywheel speed 1300r/min). The figure demonstrates a strong positive correlation between energy recovery efficiency and pump displacement. When the displacement is 10mL/r, the efficiency is only 13.4% while the efficiency increases to 53.2%, with an increase of 297% when the displacement increases to 25mL/r.

A pump with small displacement outputs a small amount of oil per revolution. The accumulator is slow accumulator charging, and most of the kinetic energy of the flywheel is loss through the internal friction and leakage of the pump; a pump with a large displacement can quickly charge the accumulator with oil, reducing energy loss, so the efficiency is significantly improved.

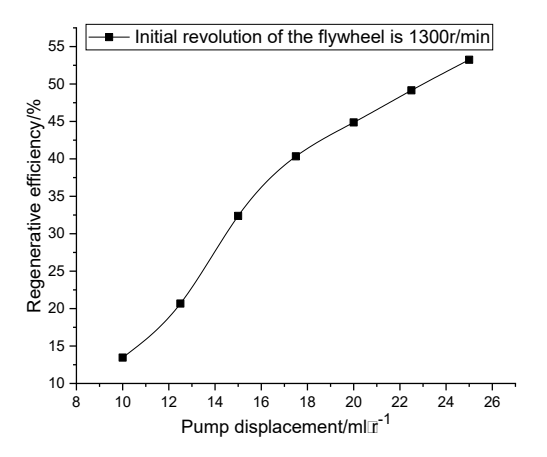


Fig. 12. Regenerative efficiency at different pump displacements.

3.3.3 Effect on energy reuse efficiency

Figure 13 shows the variation of energy reuse efficiency with the pump displacement when the initial speed is 50 km/h. The figure shows that energy reuse efficiency increases gradually with increasing pump displacement. When the displacement is 10mL/r, the efficiency is only 8.5% while the efficiency increases to 14% when the displacement is 16mL/r. The efficiency reaches the maximum value of 22% when the displacement is 25mL/r, which is 158.8% higher than the 10mL/r condition.

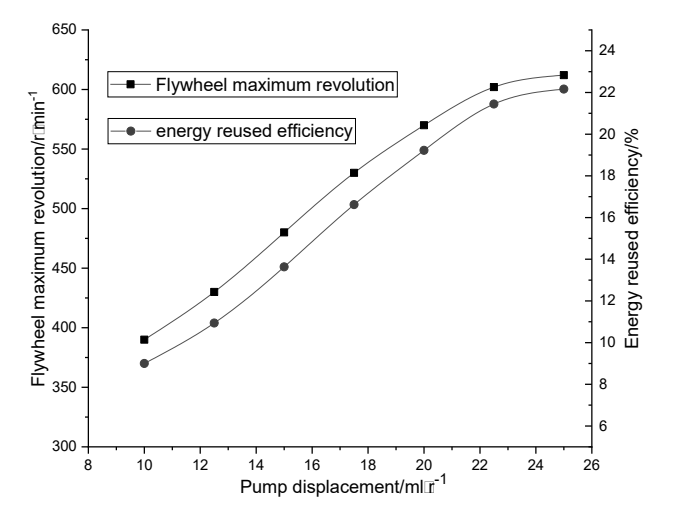


Fig. 13. Energy reused efficiency at different pump displacements.

As displacement increases, more hydraulic energy is stored in the accumulator during braking. During energy release, the accumulator can drive the flywheel to achieve higher angular velocities, enhancing kinetic energy conversion efficiency and consequently improving reuse efficiency.

4. CONCLUSION

An experimental hydraulic regenerative braking test bed was developed through structural design, component selection, and control system design. Subsequently, comprehensive experimental investigations were conducted using this test bed. The following conclusions were obtained.

- (1) The experimental results indicate that the braking energy recovery system is capable of operating independently, and the energy recovery process can be effectively evaluated under different speed conditions, demonstrating its applicability in vehicle development. Furthermore, the test bed provides significant educational value, particularly in practical teaching, by enhancing students' comprehension of the braking energy recovery system. In addition, irrespective of pump displacement, the braking distance is found to increase with the initial speed.
- (2) The regenerative efficiency depends solely on the final pressure of the accumulator and the initial vehicle speed. With increasing vehicle speed, the regenerative efficiency first rises and then declines, reaching a maximum of 58.9% at 35km/h. Moreover, under a constant initial speed, the regenerative efficiency shows a positive correlation with pump displacement. For example, when the pump displacement is 25mL/r and the initial vehicle speed is 50km/h, the regenerative efficiency reaches 53.2%.
- (3) The energy reused efficiency initially increases and then decreases with the increase in the initial rotational speed of the flywheel. The maximum energy reused efficiency reaches 35% when the initial rotational speed of the flywheel assembly is 900r/min. Simultaneously, the energy reused

- efficiency gradually increases as the pump displacement increases. The maximum energy reused efficiency can reach up to 22% when the pump displacement is 25mL/r.
- (4) The effect of hydraulic pump displacement on the braking energy recovery system involves a tradeoff, requiring a balanced consideration in practical applications.
- (5) The existing system experiences efficiency losses under both high- and low-speed working conditions due to the fixed accumulator pre-charge pressure (8.5MPa). In the future, a variable pre-charge pressure strategy can be designed to further optimize system performance across the full speed range.

ACKNOWLEDGEMENT

This work was supported by the scientific research and key project tackling initiative of Henan Province (Project No. 242102210332) and the key scientific research project of colleges and universities in Henan Province (Project No. 22B470002). The authors would like to express their appreciation for the financial support from the Power-driven Machinery and Vehicle Engineering Research Center of Henan University of Engineering.

REFERENCES

- [1] Luo C., Yang Y., and Zhong Z., 2024. Multiobjective optimization of design and control parameters for hybrid electric-hydraulic propulsion systems considering the effects of battery degradation, mass increase, and energy loss. *Energy Conversion and Management* 321: 1.1-1.15.
- [2] Khajvand F., Zareinejad M., Rezaei S.M., and Baghestan K., 2023. Design and implementation of a series hydraulic hybrid propulsion system to increase regenerative braking energy saving range. *Energy Conversion and Management* 279: 116754.1-116754.9.
- [3] Kakichi Y., Pischinger S., Schaub J., Müller A., and Kawano R., 2025. Parallel-series hybrid powertrain concept for a wheel loader. International MTZ Conference on Heavy-Duty Engines. Springer Vieweg, Wiesbaden.
- [4] Ruz-Hernandez J.A., Garcia-Hernandez R., Ruz Canul M.A., Guerra J.F., Rullan-Lara J.L., and Jaime R., 2024. Neural sliding mode control of a buck-boost converter applied to a regenerative braking system for electric vehicles. *World Electric Vehicle Journal* 15(2): 38–46.
- [5] Zhang J.Z., Lv C., Li Y.T., Gou J.F., and He C.K., 2014. Development status and prospect of braking energy recovery technology for electric-driven passenger cars. *Automotive Engineering* 36(8): 911–918.
- [6] Pourmovahed A., Beachley N.H., and Fronczak F.J., 1992. Modeling of a hydraulic energy

- regeneration system: Part II Experimental program. *Journal of Dynamic Systems, Measurement and Control* 114(1): 160–165.
- [7] Filipi Z., Louca L., Daran B., Lin C.-C., Yildir U., Wu B., Kokkolaras M., Assanis D., Peng H., Papalambros P., Stein J., Szkubiel D., and Chapp R., 2004. Combined optimization of design and power management of the hydraulic hybrid propulsion system for the 6×6 medium truck. *International Journal of Heavy Vehicle Systems* 11(3): 372–402.
- [8] Serrao L., Ornella G., Balboni L., Bort C.M.G., Dousy C., and Zendri F., 2016. A telehandler vehicle as mobile laboratory for hydraulic-hybrid powertrain technology development. 10th International Fluid Power Conference, Vol. 1, 413–424.
- [9] Ding J., 2019. Research on Design and Control of Parallel Hydraulic Hybrid Power System for Heavy-Duty Engineering Vehicles. MS Thesis, Zhejiang University, Hangzhou, China.
- [10] Zhang Y.B., Wang W.D., Zhang H., Yang C., Xiang C.L., and Li L., 2020. Research on predictive control strategy for high-efficiency braking energy recovery of hybrid electric buses based on a new improved genetic algorithm. *Journal of Mechanical Engineering* 56(18): 105–115.
- [11] Wang G., Yang K., Ma C., Wang J., Wang H.M., and Wang J.L., 2022. Research on energy management control strategy for parallel hydraulic hybrid buses. *Chinese Hydraulics & Pneumatics* 46(4): 102–109.
- [12] Zhou L.X., Ning X.B., and Xie W.D., 2013. Hydraulic regenerative braking system in electrical vehicle. *Mechanical & Electrical Engineering Magazine* 30(6): 664–668.
- [13] Zhang D.D., Zhang X.W., and Zhang W., 2015. Double accumulator for parallel hydraulic hybrid vehicle braking characteristics. *Chinese Hydraulics & Pneumatics* 45(2): 74–78.
- [14] Xu G.L., Ning X.B., and Wang N.K., 2018. Braking characteristics of the hydraulic regenerative braking system with double accumulator. *Journal of Mechanical & Electrical Engineering* 35(10): 1048-1052.
- [15] Wang T.Y., Tian Y., and Xu F.Q., 2022. Research on braking recovery of large inertia rotary mechanism based on compound electro-hydraulic systems. *Chinese Hydraulics & Pneumatics* 50(23): 99–104.
- [16] Zhang C.X., 2023. Analysis of hydraulic regenerative braking system. *Journal of The Institution of Engineers (India)*, Series C 104(6): 1141–115.
- [17] Gao S., Liu S.Q., Liu G.L., Sun R.W., Zhao J.B., Wang X.L., et al., 2025. Research on energy management strategy of oil-liquid dual-source hybrid drive telescopic handler traveling system. *International Journal of Fluid Power* 26(1): 1–17.